SETAC PRESS

Environmental Toxicology and Chemistry, Vol. 28, No. 8, pp. 1585–1591, 2009
© 2009 SETAC
Printed in the USA
0730-7268/09 $12.00 + .00

IMPACT OF KEROGEN HETEROGENEITY ON SORPTION OF ORGANIC POLLUTANTS. 1. SORBENT CHARACTERIZATION

CHEN YANG,*†§ WEILIN HUANG,‡ JIAMO FU,§ and ZHI DANG†
†School of Environmental Science and Engineering, South China University of Technology, University Town, Guangzhou 510006, China
‡Department of Environmental Sciences, Rutgers University, New Brunswick, New Jersey 08901-8551, USA
§State Key Laboratory of Organic Geochemistry, Guangzhou Institute of Geochemistry, Chinese Academy of Sciences, Wushan, Guangzhou 510640, China

(*Received* 30 *October* 2008; *Accepted* 19 *February* 2009)

Abstract—The overall goal of the present study was to establish correlations between organic pollutant sorption and physicochemical properties of kerogen materials. Three coal samples, each representing a typical kerogen type, were used as the starting materials. A thermal technique was employed to treat the kerogen materials under seven different temperatures ranging from 200 to 500°C to simulate different diagenetic history. These samples were systematically characterized for their chemical compositions, functionalities, physical rigidity, and optical properties. The results showed that the chemical, spectroscopic, and optical microscopic properties of each kerogen series changed consistently as a function of treatment temperature or kerogen maturation. The oxygen-to-carbon atomic ratio decreased from 0.29, 0.12, and 0.07 for the original lignite (XF0), fusinite (HZ0), and lopinite (LP0) samples, respectively, to 0.07, 0.06, and 0.04 for XF7, HZ7, and LP7, respectively, that underwent the highest temperature treatment. The hydrogen-to-carbon atomic ratio exhibited similar reducing trend, which is consistent with the aromaticity increasing from 45 to 58% of the original samples to 76 to 81% of highly mature samples. Under the fluorescence microscope, the organic matrix changed from yellow (original lignite sample) and red-brown (original lopinite sample) to colorless for the samples of higher maturation. The measured reflecting index increased from the original samples to the highly mature samples. Moreover, the original and the slightly matured samples exhibited very different chemical compositions and structural units among the three types due to the difference in their source materials. As the kerogen maturation increased, such differences decreased, indicating highly mature kerogen became homogenized regardless of the source material.

Keywords—Kerogen Black carbon Soil organic matter Physicochemical properties

INTRODUCTION

Soil or sediment organic matter (SOM) is an active component for the sorption of hydrophobic organic chemicals (HOCs) in surface and subsurface aquatic environments [1–3]. Weber et al. [4] first hypothesized that there are two types of physically and chemically different SOM; i.e., soft carbon or amorphous versus hard carbon or relatively condensed SOM phase. Kerogen materials, the dominant organic matrixes in coal particles and black carbon (BC), are typical examples of hard carbon materials. They may be widely found in topsoils and sediments in industrialized regions where fossil fuels are major energy sources for both industrial and domestic activities [1,5]. Several studies [5–6] reported that relative contents of kerogen and BC materials may range from a few percent to more than 80% of the total organic carbon (TOC) contents in soils and sediments.

The present study focused on characterization of physicochemical properties of kerogen materials and the impact of the kerogen properties on HOC sorption. It is well known that the physicochemical properties of SOM control both the equilibrium and the rate of HOC sorption. Due to their relatively condensed and less polar properties, hard carbon materials often exhibit greater affinities, nonlinear isotherm, and slower rates for the HOC sorption [7–10]. It is also known that, as the major organic matter in sedimentary rocks and coals, kerogen materials include an array of organic matrixes that have diverse physicochemical properties. According to geochemistry literature [11–13], kerogen can be classified to four types corresponding to four different source materials. Type I kerogen originates from algae or bacteria and is characterized by a relatively high hydrogen-to-carbon (H:C) atomic ratio (i.e., low aromaticity) and the high contents of lipid material (i.e., long-chain aliphatics). Type II kerogen originates from mixed autochthonous phytoplankton, zooplankton, and microbial organic matter and is characterized by relatively low H:C and oxygen-to-carbon (O:C) atomic ratios and moderately high aromaticity. Type III kerogen is derived from vascular plants and is characterized by a relatively high O:C atomic ratio and a high aromaticity. Black carbon, inertinite, and strongly oxidative products of type I, II, and III kerogens are categorized as type IV, which may include a combination of both charred residues of fossil fuel and biomass combustion and soot or elemental carbon condensed from incomplete fuel combustion at elevated temperature conditions. James et al. [9] reported that chars produced at different combustion temperatures from different wood materials exhibited different phenanthrene sorption properties due to the heterogeneous nature of the chars.

Kerogen materials are highly heterogeneous due to the difference in source materials and diagenetic histories. To systematically elucidate the effect of kerogen heterogeneity on the HOC sorption, it would be desired to have a set of kerogen samples that have the same source material but different diagenetic history. In the present study, we selected three types of kerogen materials as the starting organic matter and used

* To whom correspondence may be addressed (cyanggz@scut.edu.cn).
Published on the Web 5/8/2009.

a thermal simulation procedure to yield three series of variously mature kerogen materials. The thermal simulation procedure was widely used in geochemical literature for mimicking geological alterations of kerogen under laboratory conditions. The simulated kerogen materials and their parental samples were systematically characterized using different physical, chemical, and spectroscopic techniques. They were also employed as the sorbents in the latter sorption study. The results of such characterization are presented in this paper, and the equilibrium sorption data are reported in the second paper of this series [14].

MATERIALS AND METHODS

Selection of kerogen and preparation

Three coal samples, each comprising predominantly a representative kerogen type, were used as the original natural organic materials in the present study. The first coal sample was a lopinite (LP0) from Mingshan Coal Mine, Leping, Jiangxi Province, China. It contained type II kerogen with suberinite (or barkinite) as the dominant organic matrix. The second sample was a lignite (XF0) from Xianfeng Coal Mine, Kunming, Yunnan Province, China, and contained type III kerogen with vitrinite as the dominant organic matrix [15]. The third one was a fusinite (HZ0) collected from Haizhou Coal Mine, Fuxing, Liaoning Province, China. It consisted of type IV kerogen with fusinite as the dominant organic matrix. All three samples were ground to pass through a 0.5-mm diameter sieve and thermally treated at temperatures of 200, 250, 300, 350, 400, 450, and 500°C to mimic diagenesis and catagenesis of kerogen following a procedure detailed in our prior study [15]. This procedure has been widely used in coal literature for mimicking geological alterations under laboratory conditions [16]. The thermal treatment procedure generated three series of kerogen materials, each series having an identical source material but different thermal alteration histories. The treated samples of each series were labeled from 1 to 7 (e.g., HZ1) corresponding to the treatment temperatures from 200 to 500°C, respectively. These samples, along with the untreated original coal samples, were dried at 100°C under vacuum to desorb any organic volatile chemicals from the sample matrix. All 24 samples were Soxhlet-extracted with a solvent mixture of methanol to acetone to toluene at volumetric ratios of 2:3:5 for a total of 7 to 30 d until the solvents became colorless and had no fluorescence under ultraviolet lamp. The extracted samples were air-dried for 24 h and then vacuum-dried at 60°C for 10 d to eliminate the organic solvents. The 24 samples were ground, and the fraction of 63 to 100 μm diameters were retained for both characterization and sorption studies.

Elemental analysis and specific surface area measurements

All 24 samples were characterized for their physicochemical properties with chemical, microscopic, and spectroscopic methods. The organic carbon, hydrogen, oxygen, and nitrogen contents of each sample were quantified with a high temperature (>900°C) combustion method on a Heraeus elemental analyzer (CHNO-RAPID). The ash contents were determined by combustion at 950°C in a muffle furnace. The specific surface areas (SSAs) were measured using the N_2 adsorption and desorption data collected at the liquid-N_2 temperature (ASAP-1000, Micromeritics). Black carbon contents were quantified with a wet chemical oxidation method described by Song et al. [5], with which the samples were demineralized in HF + HCl acids followed by oxidation with dichromate or sulfuric acid ($K_2Cr_2O_7$ [0.1 M] + H_2SO_4 [2 M]) at 55 ± 1°C for 60 h. The BC content was calculated from the mass and TOC content of each sample before and after the oxidative treatment.

Petrographic examination

The organic petrographic properties were examined with coal petrology methods [17]. The optical slices were prepared by a standard procedure. In brief, the samples were spread on clean porcelain slides and cemented with low-fluorescence glue. After drying under the sun, the sample slides were burnished with different granular talcum powder. The sample slides were then rinsed with water and polished. The prepared sample slides were soaked with a drop of glycerol and examined under microscope (MPV-3, Leitz, Germany). The degree of maturation for the organic matrix was measured using a reflectance index of vitrinite in reflecting modes. The fluorescence features were examined in fluorescent mode with the fluorescence induced by blue light at excitation wavelength of 546 nm.

Fourier transform infrared and ^{13}C nuclear magnetic resonance

Fourier transform infrared (FTIR) spectra were obtained on a PerkinElmer 1725 X FTIR spectrometer equipped with an automatic data acquisition system. The sample pellets used were prepared by pressing a mixture of 1 mg of well-ground sample and 60 mg of infrared-grade potassium bromide.

The ^{13}C nuclear magnetic resonance (NMR) spectra were measured with Bruker DRX-400 nuclear magnetic resonance spectrometer on a 7.5-mm probe at a ^{13}C frequency of 100 MHz and a magic-angle-spinning rate of 6.0 kHz. The signals were recorded on a 1.5-ms cross-polarization contact time, and approximately 1,000 data points were obtained for each sample.

RESULTS AND DISCUSSION

Petrographic examination

Figures 1 and 2 illustrate the major features of the organic matter matrixes among samples examined with optical microscopes. Under the fluorescence mode, organic matrix with conjugated aromatic C=C and π electrons often emits fluorescence under short-wavelength radiation. The matrix with hydrogen groups such as $>CH_2$, $-OCH_3$, $-Ch_2OH$, and $-OC_2H_5$ can increase the intensity of fluorescence. As shown in Figure 1A, XF0 exhibits yellow near the edges of particles. As treated temperature increases, the color at the edges of particles changes to orange (XF1, Fig. 1B), brown (XF3, Fig. 1C), and colorlessness (XF4, Fig. 1D), indicating a gradual maturation of organic matter due to thermal alteration. For the lopinite samples, LP0 emits a red-brown color (Fig. 1E), LP1 and LP3 exhibit a light brown color (Fig. 1F and 1G), and LP4 does not emit fluorescence (Fig. 1H). The fusinite series, like the highly mature lignite and lopinite kerogen matrixes, exhibits colorlessness under fluorescence mode, indicating that these kerogen matrixes are highly carbonized and rigid. It is apparent that fluorescent intensity declines as a function of treated temperature and is finally quenched. It might be due to the delocalization of π electrons for the more maturated and aromatized organic matrix, decreasing the differences of energy level between bonding orbital and antibonding orbital and increasing the fluorescent wavelength.

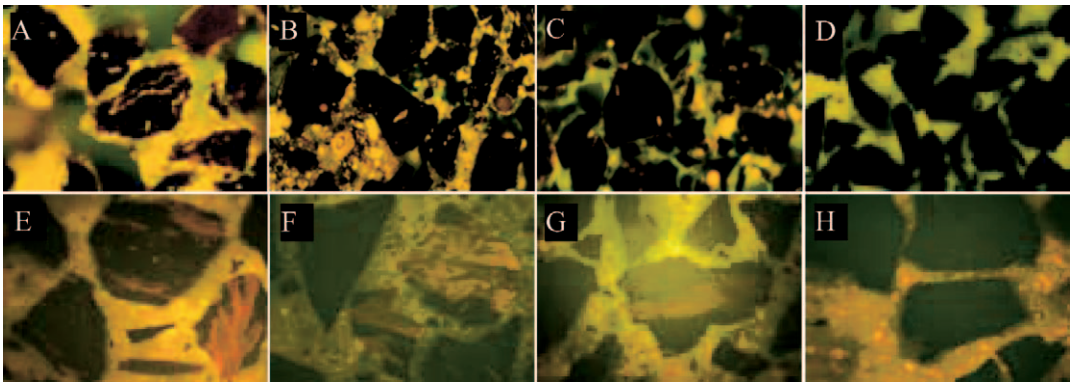

Fig. 1. Microphotographs of the lignite (XF) and lopinite (LP) samples under the fluorescent mode. (**A**) Bright orange at the edges of vitrinite in XF0. (**B**) Orange at the edges of vitrinite in XF1. (**C**) Slightly fluorescent edges of the macerals in XF3. (**D**) No fluorescence of the macerals in the XF4. (**E**) Dark brown bark structures of barkinite in LP0. (**F**) Filemot-colored bark structure of barkinite in LP1. (**G**) Filemot-colored bark structure of barkinite in LP3. (**H**) No fluorescence of the macerals in LP4. Colors can be seen in the online version of this article (http://dx.doi.org/10.1897/08-549R.1).

Under the reflecting mode, two optical features, brightness and brittleness, are indicative of the thermal maturation of organic matrix. The more thermally mature kerogen appears brighter due to greater reflection of light by the more rigid organic structures. The more rigid organic matrix also is brittle to break down during sample preparation, resulting in rough surfaces and irregular shapes. Meanwhile, high temperature can cause evaporation of volatile organic constituents, leaving pores within the matrix. For the lignite series, vitrinite is the dominant maceral. It changes from a gray color with smooth surfaces and regular shapes of XF0 (Fig. 2A) to a bright color with rough surfaces and an irregular shape of XF7 (Fig. 2D) as the thermal treatment temperature increases. Similar trends can be seen for the organic matrixes of the lopinite series, in which barkinite, the dominant maceral of the lopinite samples, is characterized by bark structure preserved in LP0 (Fig. 2E). As the treated temperature increases, the bark structure disappears and the organic matrix becomes brighter in LP3 and LP4 (Fig. 2F and G). At the highest treatment temperature, the organic matrix (LP7) becomes porous (Fig. 2H) due to evaporation of volatile moieties. Fusinite, the dominant maceral of the fusinite series, contains the preserved plant cell structure in HZ0 to HZ7 (Fig. 2I to L) and pyrofusinite with yellow color in HZ5 and HZ7 (Fig. 2K and L).

Table 1 lists the reflectivity index of vitrinite, R°, an indicator by which the greater R° value is correlated to the more mature organic matrix. According to Table 1, as treatment temperature increases, the three series of kerogen materials all become more mature. The measured R° value increases from 0.3% for XF0 to 2.6% for XF7. Similarly, the R° value increases from 0.61 to 3.03% for LP0 to LP7 and from 0.56 to 3.11% for HZ0 to HZ7. These samples have a complete spectrum of kerogen with geochemical alterations from early diagenesis ($R° < 0.6\%$), to late diagenesis ($R° = 1.4–1.7\%$), to

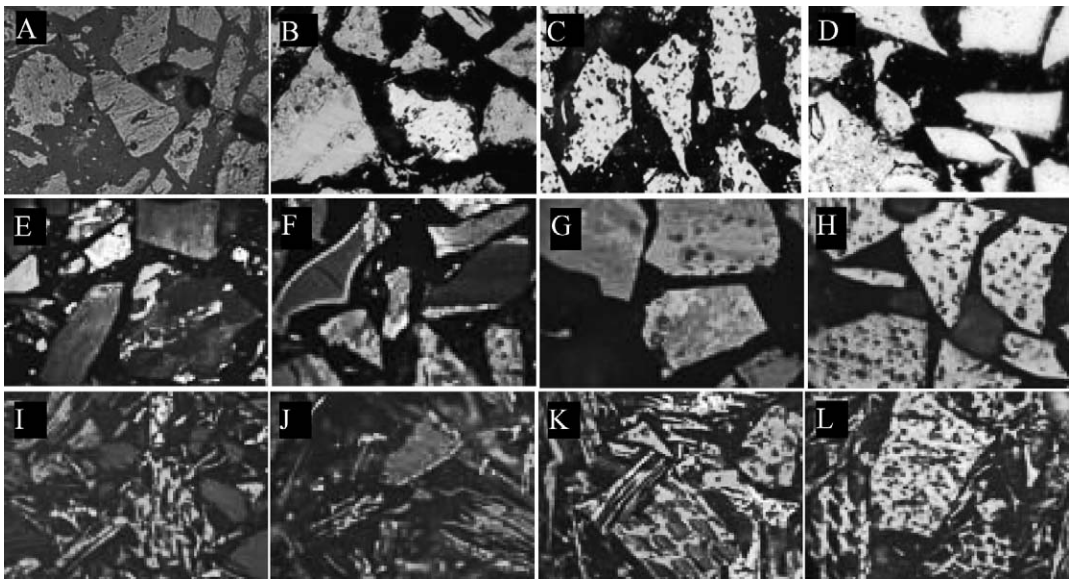

Fig. 2. Microphotographs of the lignite (XF), lopinite (LP) and fusinite (HZ) samples under the reflecting mode. (**A**) Vitrinite in XF0. (**B**) Fusinite with high reflectance (**center**) and vitrinite with low reflectance in XF4. (**C**) Fusinite with irregular dark-colored pores in XF6. (**D**) Vitrinite with high reflectance in XF7. (**E**) Gray bark structure of barkinite in LP0. (**F**) Barkinite (**right**) and thermal edge of vitrinite in LP3. (**G**) Barkinite with high reflectance in LP4. (**H**) Barkinite with high reflectance and dark-colored pores in LP7. (**I**) Vitrinite with gray fusinite with cell structure and high reflectance in HZ0. (**J**) Fusinite segments and vitrinite with thermal edge in HZ3. (**K**) Fusinite segments and cell structure in HZ5. (**L**) Vitrinite with high reflectance and dark-colored pores and fusinite with high reflectance in HZ7.

Table 1. The properties of 24 sorbents[a]

Sample	Treat temp °C	Elemental composition % C	N	H	O	Ash wt %	Atomic ratio O:C	H:C	BC wt %	SSA-N_2 m^2/g	R° %
Lignite											
XF0	Original	60.4	1.76	4.76	23.0	2.58	0.29	0.95	ND	4.50	0.31
XF1	200	62.3	2.12	4.85	22.7	2.74	0.27	0.93	ND	6.04	0.38
XF2	250	64.3	2.05	4.71	20.9	2.86	0.24	0.88	ND	2.69	0.46
XF3	300	65.4	1.09	5.50	19.6	3.04	0.22	1.01	ND	3.79	0.59
XF4	350	69.9	2.47	5.53	16.3	3.51	0.18	0.95	ND	4.71	0.86
XF5	400	75.0	2.72	4.64	13.3	3.86	0.13	0.74	ND	7.69	1.42
XF6	450	77.9	2.70	4.46	10.1	4.21	0.10	0.69	76.9	10.7	2.07
XF7	500	80.9	2.66	3.67	7.30	4.54	0.07	0.54	80.0	17.1	2.61
Lopinite											
LP0	Original	76.3	1.91	5.56	6.72	8.72	0.07	0.87	71.2	0.61	0.61
LP1	200	76.4	1.61	4.52	7.01	9.20	0.07	0.71	—	0.52	0.63
LP2	250	76.7	1.77	4.83	7.18	8.91	0.07	0.75	—	—	0.67
LP3	300	76.9	1.18	5.55	7.73	8.84	0.08	0.87	73.3	0.51	0.69
LP4	350	76.6	1.96	3.70	7.11	9.30	0.07	0.58	—	—	1.05
LP5	400	78.9	1.81	3.47	5.90	10.0	0.06	0.53	80.7	0.52	1.79
LP6	450	78.8	0.78	2.46	4.77	10.5	0.05	0.37	—	—	2.44
LP7	500	80.3	1.80	2.74	4.04	10.5	0.04	0.41	90.9	0.83	3.03
Fusinite											
HZ0	Original	75.1	0.59	4.38	12.3	6.68	0.12	0.70	59.7	1.49	0.56
HZ1	200	74.8	0.75	3.99	12.4	6.89	0.12	0.64	—	NA	0.59
HZ2	250	76.9	1.17	4.90	13.4	6.59	0.13	0.76	—	NA	0.70
HZ3	300	76.3	0.87	3.83	12.4	6.87	0.12	0.60	64.7	NA	0.76
HZ4	350	78.3	0.52	3.50	11.2	6.45	0.11	0.54	—	NA	0.92
HZ5	400	81.1	1.08	3.57	8.95	6.60	0.08	0.53	78.7	NA	1.69
HZ6	450	83.7	0.75	3.70	6.07	7.24	0.05	0.53	—	NA	2.53
HZ7	500	83.9	0.75	3.4	6.44	7.09	0.06	0.49	91.3	29.7	3.11

[a] Treat temp = treatment temperature; O:C = oxygen-to-carbon atomic ratio; H:C = hydrogen-to-carbon atomic ratio; BC = black carbon; SSA = specific surface area; R° = reflectivity index of vitrinite; ND = not detected; — = not measured; NA = not available.

metagenesis (R° > 2.5%) [12,17]. It should be noted that the original and less altered samples of the lopinite and fusinite series have approximately similar R° values (0.61–0.69% for LP0–LP3 and 0.56–0.70% for HZ0–HZ2). These values are close to that of XF3 (~0.59%), suggesting that the original lopinite and fusinite samples have a greater degree of maturation than the original lignite sample and that the lower treatment temperature (<300°C) under laboratory conditions might have little or no effect on the organic matrix.

Chemical characteristics

The chemical characterization indicates that thermal maturation process may eliminate oxygen-containing and aliphatic functional groups, resulting in graphitization and deoxygenation of the organic matrix. Table 1 lists the elemental composition, O:C and H:C atomic ratios, and BC content for each kerogen sample. It shows that both TOC and ash contents for lignite samples increase and oxygen content decreases as a function of the treatment temperature. The organic nitrogen and hydrogen contents remain relatively constant among the sample series. The H:C atomic ratios remained relatively constant from 0.88 to 1.01 for the first five samples (XF0–XF4) and then decreased to 0.54 (XF7), suggesting that, at 350°C or higher, aliphatic chains were eliminated from organic matrix, resulting in more aromatic kerogen structures.

The lopinite and fusinite sample series exhibit similar changes of elemental compositions and O:C and H:C atomic ratios, except that the ranges of the TOC contents are narrower due to higher TOC contents of the more mature original lopinite and fusinite samples. Meanwhile, the oxygen contents of lopinite series are relatively constant (4.04 to 6.72% weight concentration) as treatment temperature increases. It is interesting to note that the most mature XF7, LP7, and HZ7 have similar H:C (0.41–0.54) and O:C (0.04–0.07) atomic ratios even though their original organic materials differ dramatically. This suggests that the highly mature organic matrixes become carbonized BC that is structurally and chemically similar regardless of its parental matter.

Black carbon content

For the lignite series, the BC contents on a TOC basis vary from being not measurable for the low-maturity samples to about 80% for the two treated at 450 and 500°C. The samples of both lopinite and fusinite series contained BC, and the measured BC contents increased from approximately 60 to 70% for the original samples (LP0 and HZ0) to above 90% for the two samples treated at 500°C (LP7 and HZ7). The results further indicate that the starting lopinite and fusinite samples are more mature compared to the original lignite sample. This is consistent with the measured reflectivity values of vitrinite (Table 1). It should be noted that the samples treated at 450 and 500°C should have been converted to char or BC but that the measured BC contents were all lower than 100%. This is likely due to sample loss, partial oxidation of BC particles, or both during BC measurement [5].

Specific surface area

For the lignite series, the measured SSA decreased initially and then increased as a function of treatment temperature. The initial decrease of SSA is likely caused by shrinkage of internal pores due to expanding of aliphatic chains to a fluidal state [15] under moderate thermal treatment conditions. As treat-

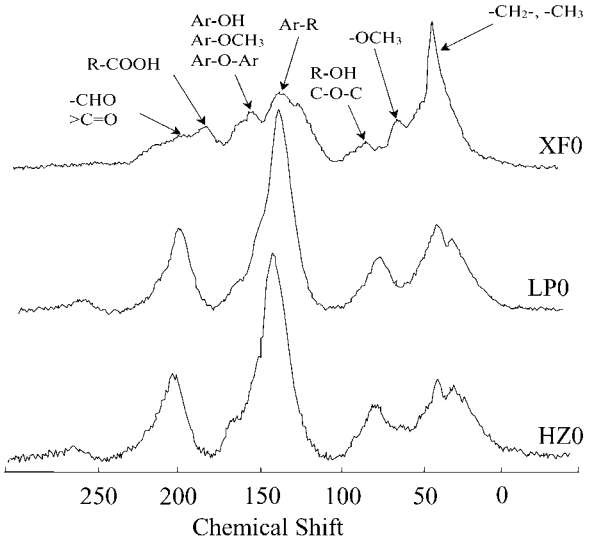

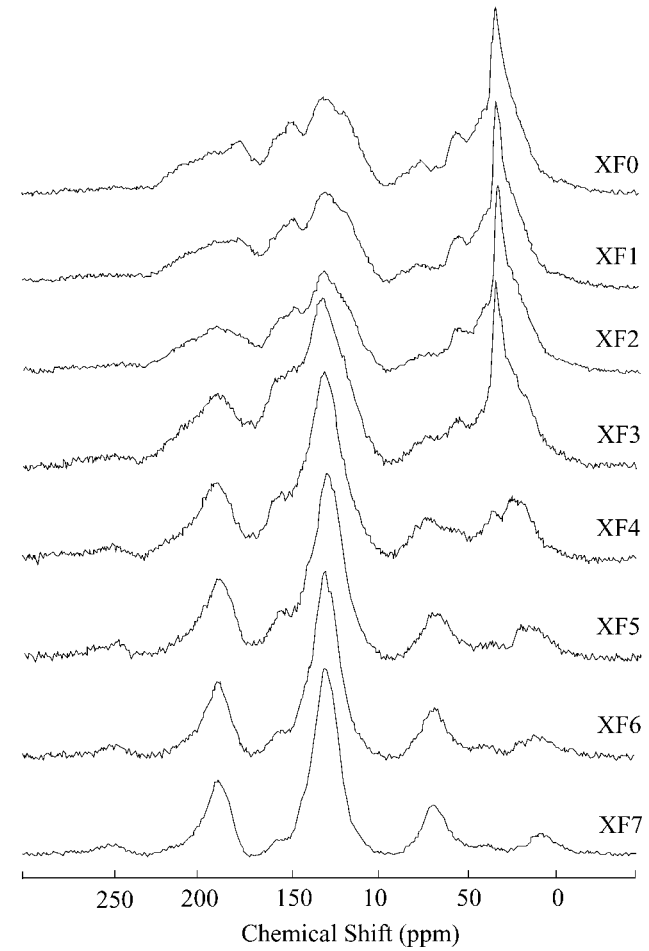

Fig. 3. ^{13}C nuclear magnetic resonance spectra of original lignite (XF0), lopinite (LP0), and fusinite (HZ0) samples (**upper**) and XF series (**lower**).

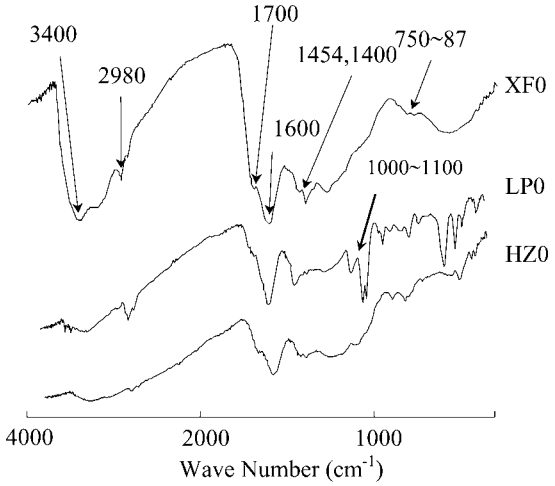

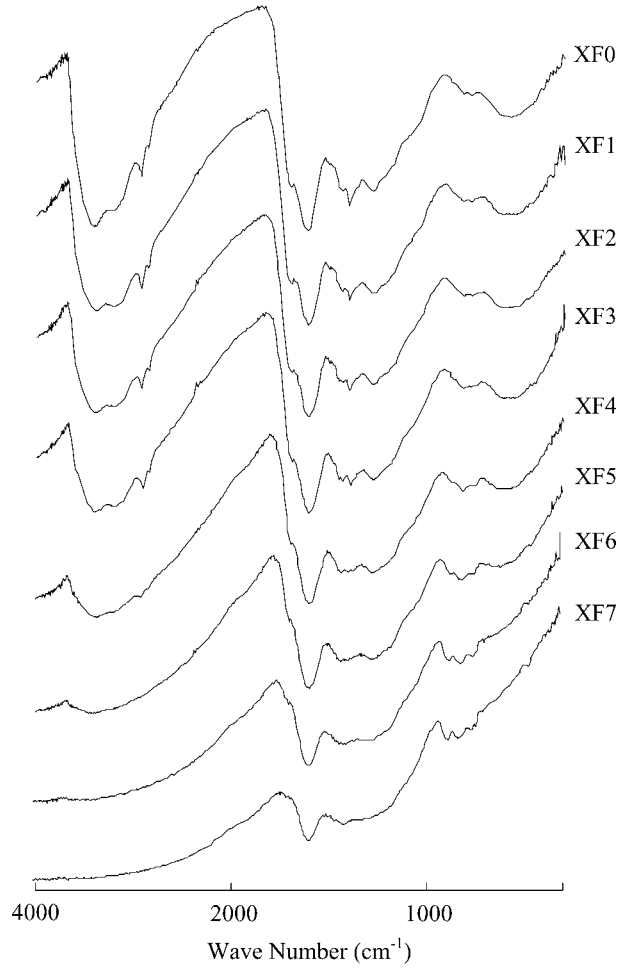

Fig. 4. Fourier transform infrared spectra of original lignite (XF0), lopinite (LP0), and fusinite (HZ0) samples (**upper**) and XF series (**lower**).

ment temperature increased, the oxygen-containing functional groups and aliphatic groups cracked and evaporated, yielding more porous matrixes.

The lopinite series has relatively constant SSA values of 0.51 to 0.83 m^2/g, which are lower than the lignite samples. The lowered SSA is likely due to higher contents of aliphatic and oxygen-bridge structures in lopinite samples. The SSA was measured only for HZ0 (1.49 m^2/g) and HZ7 (29.7 m^2/g) because of insufficient mass for other six fusinite samples. The two data points appear to be consistent with the data for the lignite series.

^{13}C nuclear magnetic resonance spectra

Solid-state ^{13}C NMR spectra are shown in Figures 3 and S1 for the three series, respectively. The contents were calculated from the relative abundance of each peak of the relative

Table 2. Contents of functional groups by ^{13}C nuclear magnetic resonance[a]

Sample	Aliphatic 0–45 ppm	Methoxyl 45–63 ppm	Carbohydrate 63–93 ppm	Aromatic 93–148 ppm	Aromatic[b] 148–165 ppm	Carboxyl 165–187 ppm	Carbonyl 187–220 ppm	f_a[c] %
Lignite								
XF0	33.1	7.36	4.75	25.1	11.7	8.63	9.34	44.9
XF1	33.7	7.06	3.51	25.7	12.5	8.44	9.15	46.3
XF2	33.4	7.19	2.58	26.5	11.8	6.48	12.1	47.0
XF3	25.5	5.13	3.36	29.2	17.4	—	19.3	57.8
XF4	16.7	3.73	7.26	44.3	8.65	—	19.4	65.7
XF5	8.16	—	10.7	50.5	7.77	—	22.9	75.5
XF6	5.51	—	12.1	58.4	3.84	—	20.2	77.9
XF7	4.99	—	10.6	62.0	2.28	—	20.1	80.5
Lopinite								
LP0	27.84	—	11.06	41.95	3.37	—	15.79	53.81
LP3	24.5	—	13.2	42.98	2.92	—	16.39	54.91
LP5	10.12	—	15.09	60.41	—	—	14.38	70.56
LP7	5.4	—	13.45	60.91	—	—	20.24	76.37
Fusinite								
HZ0	24.07	—	9.92	43.57	4.26	—	18.18	58.46
HZ3	20.14	—	9.53	47.57	4.07	—	18.69	63.51
HZ5	6.69	—	12.59	57.86	3.28	—	19.57	76.02
HZ7	4.81	—	13.37	60.29	1.77	—	19.76	77.34

[a] ppm = parts per million; — = not measured.
[b] Oxygen-substituted aromatics.
[c] Aromaticity (f_a) is the ratio of the peak area integrated over 93 to 165 ppm as the aromatic carbon region to that over 0 to 165 ppm as the total carbon region.

contents of major functional groups listed in Table 2. For the original lignite sample, there are seven major resonance peaks that can be assigned to aliphatic carbon (0–45 ppm), methoxyl carbon (45–63 ppm), carbohydrate carbon (63–93 ppm), aromatic carbon (93–148 ppm), oxygen-substituted aromatic carbon (148–165 ppm), carboxyl carbon (165–187 ppm), and carbonyl carbon (187–220 ppm). As the treatment temperature increases, the peak areas of aromatic, carbohydrate, and carbonyl carbon increase, whereas the peak areas for aliphatic, oxygen-substituted aromatic, methoxyl, and carboxyl carbon decrease. For the more mature lignite (XF7), aromatic carbon is the dominant peak and methoxyl and carboxyl carbon disappeared. For the lopinite and fusinite sample series, both original samples have four major resonance peaks: aliphatic carbon (0–45 ppm), carbohydrate carbon (63–93 ppm), aromatic carbon (93–148 ppm), and carboxyl carbon (165–187 ppm). Within the aliphatic carbon region, there are two separate peaks corresponding to methyl groups (14–25 ppm) and methylene groups (25–45 ppm; i.e., R-CH_3, Ar-CH_3, –CH_2–). The oxygen-substituted groups (45–63 ppm and 148–165 ppm), which are present in both lignite and fusinite samples, are not shown on the spectra obtained for the original lopinite sample, consistent with the low oxygen content of the sample. The spectra of the three most mature samples (XF7, LP7, and HZ7) are nearly identical, suggesting that, regardless of their source materials, organic matrixes become structurally and chemically similar with aromatic carbon as the major structures.

Aromaticity (f_a) was calculated based on the ratio of peak areas integrated from 93 to 165 ppm to those from 0 to 165 ppm. According to Table 2, the f_a value increases from 45, 54, and 58% for XF0, LP0, and HZ0 to 80, 76, and 77% for XF7, LP7, and HZ7, respectively. This trend is consistent with the changes of elemental composition and optical properties of the samples.

Fourier transform infrared spectra

The FTIR spectra are shown in Figures 4 and S2 for the three series. For the lignite series, the FTIR spectra include hydrogen-bonded O–H stretching vibration at 3,400 cm^{-1}, asymmetric and symmetric stretching vibration of aliphatic C–H at 2,980 cm^{-1}, stretching vibration of aromatic carbonyl/carboxyl C=O at 1,700 cm^{-1}, stretching vibration of conjugated aromatic C=C at 1,600 cm^{-1}, deformation vibration of aliphatic and branched aliphatic C–H at 1,454 and 1,400 cm^{-1}, and C–H bending of aromatic ring at 750 to 870 cm^{-1} [11,18]. As treatment temperature increases, the peak of aliphatic carbon shrinks whereas the peak of aromatic carbon increases gradually. This is consistent with ^{13}C NMR spectra and chemical characteristics of the samples, indicating that the aliphatic carbons and the other substituted groups on aromatic rings were removed upon heating.

The lopinite and fusinite series samples display similar characteristics of FTIR spectra. One exception is that the original lopinite sample had a peak at 1,000 to 1,100 cm^{-1}, resulting from the stretching vibration of C–O–C, which is indicative of the presence of aliphatic ether C–O–C and alcohol C–O structures [19]. The spectra of the three most mature samples are nearly identical, suggesting that the organic matrixes become chemically and structurally similar as revealed by the ^{13}C NMR spectra.

CONCLUSION

The chemical and spectral characteristics of the present study indicate that the original and the slightly mature kerogen samples exhibited various differences in chemical compositions and structural units, that the aromaticity and rigidity of each series of the kerogen materials increased as a function of treatment temperature and hence maturation, and that the most mature kerogen materials had similar properties. This suggests that kerogen particles found in soils and sediments

may have a range of physicochemical properties and should not be considered as a single organic phase. The sorption properties may also differ greatly among the kerogen particles with different maturation and source materials.

SUPPORTING INFORMATION

Fig. S1. ^{13}C nuclear magnetic resonance spectra of lopinite (LP) and fusinite (HZ) series.

Fig. S2. Fourier transform infrared spectra of lopinite (LP) and fusinite (HZ) series samples.

All found at DOI: 10.1897/08-549.S1 (47 KB PDF).

Acknowledgement—The authors thank Dehan Liu and Jialan Lu of the Guangzhou Institute of Geochemistry, Chinese Academy of Sciences, for their assistance in petrographic examinations and thermal treatment of the sorbent materials, respectively. The present study was funded by the Natural Science Foundation of China (40502031) and Natural Science Foundation of Guangdong Province (05300187). Partial funding was also provided by the Chinese Academy of Sciences, New Jersey Water Resource Research Institute, and Multistate Project (W-1082) from the U.S. Department of Agriculture Cooperative State Research, Education, and Extension Service to W. Huang.

REFERENCES

1. Huang WL, Peng PA, Yu ZQ, Fu JM. 2003. Effects of organic matter heterogeneity on sorption and desorption of organic contaminants by soils and sediments. *Appl Geochem* 18:955–972.
2. Chiou CT, Peters LJ, Freed VH. 1979. A physical concept of soil–water equilibria for non-ionic organic compounds. *Science* 206: 831–832.
3. Huang WL, Weber WJ Jr. 1997. A distributed reactivity model for sorption by soils and sediments. 10. Relationships between sorption, hysteresis, and the chemical characteristics of organic domains. *Environ Sci Technol* 31:2562–2569.
4. Weber WJ Jr, McGinley PM, Katz LE. 1992. A distributed reactivity model for sorption by soils and sediments. 1. Conceptual basis and equilibrium assessments. *Environ Sci Technol* 26:1955–1962.
5. Song JZ, Peng PA, Huang WL. 2002. Black carbon and kerogen in soils and sediments. 1. Quantification and characterization. *Environ Sci Technol* 36:3960–3967.
6. Accardi-Dey A, Gschwend PM. 2002. Assessing the combined roles of natural organic matter and black carbon as sorbents in sediments. *Environ Sci Technol* 36:21–29.
7. Cornelissen G, Gustafsson Ö. 2005. Importance of unburned coal carbon, black carbon, and amorphous organic carbon to phenanthrene sorption in sediments. *Environ Sci Technol* 39:764–769.
8. Koelmans AA, Jonker MTO, Cornelissen G, Bucheli TD, van Noort PCM, Gustafsson Ö. 2006. Black carbon: The reverse of its dark side. *Chemosphere* 63:365–377.
9. James G, Sabatini DA, Chiou CT, Rutherford D, Scott AC, Karapanagioti HK. 2005. Evaluating phenanthrene sorption on various wood chars. *Water Res* 39:549–558.
10. Kleineidam S, Rügner H, Grathwohl P. 1999. Influence of petrographic composition/organic matter distribution of fluvial aquifer sediments on the sorption of hydrophobic contaminants. *Sediment Geol* 129:311–325.
11. Durand B. 1980. *Kerogen: Insoluble Organic Matter from Sedimentary Rocks.* Technip, Paris, France.
12. Tissot BP, Welte DH. 1984. *Petroleum Formation and Occurrence.* Springer-Verlag, New York, NY, USA.
13. Brooks J. 1981. Organic maturation of sedimentary organic matter and petroleum exploration: A review. In Brooks J, ed, *Organic Maturation Studies and Fossil Fuel Exploration.* Great Yarmouth, London, UK, pp 1–37.
14. Yang C, Yu ZQ, Xiao BH, Huang WL, Fu JM, Dang Z. 2009. Impact of kerogen heterogeneity on sorption of organic pollutants. 2. Sorption equilibria. *Environ Toxicol Chem* 28:1592–1598.
15. Yang C, Huang WL, Xiao BH, Yu ZQ, Peng PA, Fu JM, Sheng GY. 2004. Intercorrelations among degree of geochemical alterations, physicochemical properties, and organic sorption equilibria of kerogen. *Environ Sci Technol* 38:4396–4408.
16. Saxby JD, Bennett JR, Corcoran JF, Lambert DE, Riley KW. 1986. Petroleum generation: Simulation over six years of hydrocarbon formation from torbanite and brown coal in a subsiding basin. *Org Geochem* 9:69–81.
17. Stach E, Mackowsky M, Teichmuller M, Taylor GH, Chandra D, Teichmuller R. 1982. *Coal Petrology.* Gebruder Borntraeger, Berlin, Germany.
18. Guo YT, John JR, John HP. 1996. FTIR microspectroscopy of particular lopinite (lopinite)–rich, late Permian coals from South China. *Int J Coal Geol* 29:187–197.
19. Sun XG. 2005. The investigation of chemical structure of coal macerals via transmitted-light FT-IR microspectroscopy. *Spectrochim Acta Part A* 62:557–564.